Compressed ghost edge imaging

Hui Guo (郭 辉)[1,2], Ruyong He (何儒勇)[1], Chaopeng Wei (魏朝鹏)[1], Zequn Lin (林泽群)[1], Le Wang (王 乐)[1], and Shengmei Zhao (赵生妹)[1,*]

[1]*Institute of Signal Processing and Transmission, Nanjing University of Posts and Telecommunications, Nanjing 210003, China*

[2]*College of Information Engineering, Fuyang Normal University, Fuyang 236037, China*

**Corresponding author: zhaosm@njupt.edu.cn*

Received February 21, 2019; accepted April 18, 2019; posted online July 1, 2019

In this Letter, we propose an advanced framework of ghost edge imaging, named compressed ghost edge imaging (CGEI). In the scheme, a set of structured speckle patterns with pixel shifting illuminate on an unknown object. The output is collected by a bucket detector without any spatial resolution. By using a compressed sensing algorithm, we obtain horizontal and vertical edge information of the unknown object with the bucket detector detection results and the known structured speckle patterns. The edge is finally constructed via two-dimensional edge information. The experimental and numerical simulations results show that the proposed scheme has a higher quality and reduces the number of measurements, in comparison with the existing edge detection schemes based on ghost imaging.

OCIS codes: 110.1650, 110.1758.
doi: 10.3788/COL201917.071101.

Ghost imaging (GI), also called single-pixel imaging, is a novel optical imaging technique that has received great attention recently[1–5]. There are two spatially correlated optical beams in a GI system. One beam, called the object beam, illuminates an unknown object, and the resulting scattered light is then collected by a bucket detector without any spatial resolution. The other beam, named the reference beam, never interacts with the object and is detected by a spatially resolving detector. A ghost image is reconstructed by correlating the bucket signal and the reference signal, but not either one alone. Compared with traditional imaging methods, GI can be used to reconstruct the image of the object in various optically harsh or noisy environments[6].

Edge detection methods find edges by noticing dramatic changes in image processing. It is extensively used in image segmentation, target recognition, and computer vision[7,8]. In traditional edge detection methods, the object needs to be imaged first, and the edge information can be obtained by developing a corresponding edge operator. However, in harsh or noisy environments, the imaging step is difficult to achieve, so the edge detection algorithm cannot be implemented. Given the special properties of GI, edge detection methods based on GI can solve the problem of disturbances in the optical path and have an advantage in edge detection. In recent years, GI-based edge detection has achieved some results[9–13]. In Ref. [9], a gradient GI (GGI) was proposed to detect edges of an unknown object directly. However, it is a problem for choosing a proper gradient angle based on the prior knowledge of the object in this method. Subsequently, speckle-shifting GI (SSGI) was introduced to find the edge of an unknown object without additional prior knowledge of the object[10]. Meanwhile, subpixel-SSGI was proposed, which can enhance the resolution of edge detection with low resolution speckle patterns[11]. In Ref. [12], the authors presented structured intensity patterns to find the edge of an object directly from the data detected by computational GI (CGI). In Ref. [13], special sinusoidal patterns were designed to find the edge of an unknown object with an improvement in the signal-to-noise ratio (SNR) in the frequency domain. However, the number of measurements of these schemes is large, and the quality of the edge detection results still needs to be improved.

On the other hand, a compressed sensing (CS) method was introduced into GI to obtain a higher resolution image of an object by exploiting the redundancy in the structure of the images to reduce the number of measurements required for exact reconstruction[14–16]. Therefore, a GI method based on CS can enable the reconstruction of an N-pixel image from much less than N measurements, which overcomes the limitations of the Nyquist sampling theorem and greatly reduces the acquisition time and number of required measurements[17,18].

In the Letter, we propose a GI-based edge detection scheme that combines selected features of a CS technique. We call our method compressed ghost edge imaging (CGEI). In the scheme, special random patterns with characteristics of different speckle-shifting are first designed. In the CS technique, high-quality horizontal and vertical edge information could be obtained directly from the bucket detector detection results and the structured illuminations. Lastly, the global edge of the unknown object is constructed with two-dimensional edge information.

Figure 1 shows the schematic diagram of the CGEI scheme. The light is modulated by a digital micro-mirror device (DMD), which is controlled by a computer to produce the speckle patterns $S_k(x_i, y_j)$, $k = 1, 2, ..., M$, where M is the number of speckle patterns, and x_i, y_j are the spatial coordinates. The bucket detector measures the

total light transmitted by the object $T(x_i, y_j)$, and the output signal is detected as

$$y_k = \sum_{x_i} \sum_{y_j} S_k(x_i, y_j)\, T(x_i, y_j), \tag{1}$$

where $S_k(x_i, y_j)$ can be pre-designed. The image of the object can be obtained by applying a second-order correlation[9],

$$T(x_i, y_j) = \langle S_k(x_i, y_j) \cdot y_k \rangle - \langle S_k(x_i, y_j) \rangle \langle y_k \rangle, \tag{2}$$

where $\langle \cdot \rangle$ denotes the ensemble average.

Speckle-shifting, introduced by an edge operator (such as gradient vector and Sobel operator), automatically detects the edge of an unknown object[9,10]. In this work, we use the Sobel operator to introduce the principle of CGEI. To achieve edge detection, several speckle groups are divided, and they are related as follows:

$$\begin{aligned} S_k(x_i, y_j) &= S_k^1(x_{i-1}, y_{j-1}) = S_k^2(x_{i-1}, y_j) = S_k^3(x_{i-1}, y_{j+1}) \\ &= S_k^4(x_i, y_{j-1}) = S_k^5(x_i, y_{j+1}) = S_k^6(x_{i+1}, y_{j-1}) \\ &= S_k^7(x_{i+1}, y_j) = S_k^8(x_{i+1}, y_{j+1}), \end{aligned} \tag{3}$$

where S_k^l, $l = 1, 2, ..., 8$ represents the lth group of shifted speckle patterns. By using the Sobel operator property and Eq. (1), one obtains the horizontal measurements as follows:

$$\begin{aligned} \nabla y_k^h &= \sum_{x_i} \sum_{y_j} S_k^1(x_i, y_j)\, T(x_i, y_j) \\ &\quad + 2 \times \sum_{x_i} \sum_{y_j} S_k^2(x_i, y_j)\, T(x_i, y_j) \\ &\quad + \sum_{x_i} \sum_{y_j} S_k^3(x_i, y_j)\, T(x_i, y_j) \\ &\quad - \sum_{x_i} \sum_{y_j} S_k^6(x_i, y_j)\, T(x_i, y_j) \\ &\quad - 2 \times \sum_{x_i} \sum_{y_j} S_k^7(x_i, y_j)\, T(x_i, y_j) \\ &\quad - \sum_{x_i} \sum_{y_j} S_k^8(x_i, y_j)\, T(x_i, y_j) \\ &= \sum_{x_i} \sum_{y_j} S_k(x_i, y_j)[T(x_{i-1}, y_{j-1}) + 2 \times T(x_{i-1}, y_j) \\ &\quad + T(x_{i-1}, y_{j+1}) - T(x_{i+1}, y_{j-1}) \\ &\quad - 2 \times T(x_{i+1}, y_j) - T(x_{i+1}, y_{j+1})] \\ &= \sum_{x_i} \sum_{y_j} S_k(x_i, y_j) \nabla_h^S T(x_i, y_j), \end{aligned} \tag{4}$$

where $\nabla_h^S T(x_i, y_j)$ represents the horizontal edge of the unknown object using the Sobel operator. Using Eq. (2), the horizontal edge of the object is

$$\nabla_h^S T(x_i, y_j) = \langle S_k(x_i, y_j) \cdot \nabla y_k^h \rangle - \langle S_k(x_i, y_j) \rangle \langle \nabla y_k^h \rangle; \tag{5}$$

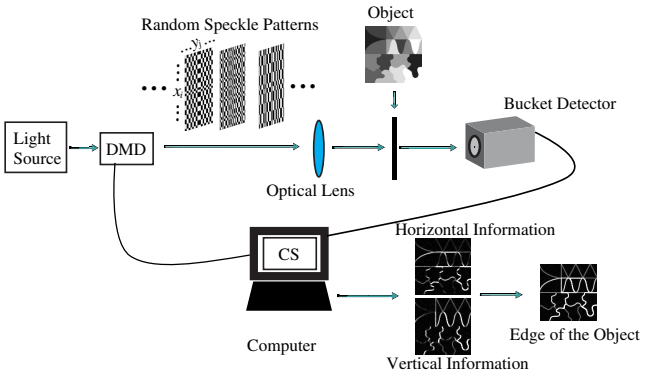

Fig. 1. Schematic diagram of the CGEI scheme.

similarly, the vertical edge of the object is obtained as

$$\nabla_v^S T(x_i, y_j) = \langle S_k(x_i, y_j) \cdot \nabla y_k^v \rangle - \langle S_k(x_i, y_j) \rangle \langle \nabla y_k^v \rangle, \tag{6}$$

where ∇y_k^v represents vertical measurements, and $\nabla_v^S T(x_i, y_j)$ represents the vertical edge of an unknown object using a Sobel operator. Finally, the edge of the object will be obtained by

$$T_{\text{edge}} = \sqrt{[\nabla_h^S T(x_i, y_j)]^2 + [\nabla_v^S T(x_i, y_j)]^2}. \tag{7}$$

Although the above method can reconstruct the edge of an unknown object, too many measurements are needed. However, any prior information using the structure of an object, such as sparsity, could reduce the number of measurements required for a faithful reconstruction. It is demonstrated that CS algorithms allow us to get good reconstructions for GI, provided that the number of measurements is smaller than the number of pixels of the image[16–18]. The edge images of the object are sparse, that is, most pixels of the edge images are zero. Thus, we can introduce the CS method in ghost edge imaging to reduce the number of measurements needed for faithful edge detection even though they suffer from some computational overhead. In this work, we adopt the total variation minimization by augmented Lagrangian and alternating direction algorithms (TVAL3)[19]. The speckle field of the kth sample is recorded as $S_k(x_i, y_j)$. The index x_i represents the horizontal pixel coordinate and $i = 1, 2, ..., m$; the index y_j represents the vertical pixel coordinate and $j = 1, 2, ..., n$. The k values represent the sampling frame index, and M is the total number of speckle patterns. Next, each speckle intensity $S_k(x_i, y_j)$ is reshaped as a row vector $\boldsymbol{\phi}_k$ of size $1 \times N$, where $N = n \times m$,

$$\begin{aligned} \boldsymbol{\phi}_k = [&S_k(x_1, y_1) \quad \cdots \quad S_k(x_1, y_n) \quad S_k(x_2, y_1) \quad \cdots \\ &S_k(x_2, y_n) \quad \cdots \quad S_k(x_m, y_1) \quad \cdots \quad S_k(x_m, y_n)]; \end{aligned} \tag{8}$$

after M samples, we can get an $M \times N$ samples array recorded as A, and it can be written as the following matrix:

$$A = \begin{bmatrix} \phi_1 \\ \phi_2 \\ \vdots \\ \phi_M \end{bmatrix} = \begin{bmatrix} S_1(x_1, y_1) & S_1(x_1, y_2) & \cdots & S_1(x_m, y_n) \\ S_2(x_1, y_1) & S_2(x_1, y_2) & \cdots & S_2(x_m, y_n) \\ \vdots & \vdots & & \vdots \\ S_M(x_1, y_1) & S_M(x_1, y_2) & \cdots & S_M(x_m, y_n) \end{bmatrix}. \quad (9)$$

The signal from the bucket detector, containing horizontal information of the unknown object, can be arranged as an $M \times 1$ column vector Y^h, i.e., $Y^h = [\nabla y_1^h \ \nabla y_2^h \ \cdots \ \nabla y_k^h \ \cdots \ \nabla y_M^h]^T$. Taking ∇y_k^h for example, it can be obtained by

$$\nabla y_k^h = y_k^1 + 2 \times y_k^2 + y_k^3 - y_k^6 - 2 \times y_k^7 - y_k^8, \quad (10)$$

where y_k^l, $l = 1, 2, 3, 6, 7, 8$ is the bucket value corresponding to S_k^l, $l = 1, 2, 3, 6, 7, 8$ passing through the unknown object. Therefore, $\nabla_h^S T(x_i, y_j)$ could be reconstructed as a solution[19]:

$$\min \sum_f \| D_f X^h \|_1 + \frac{\mu}{2} \| Y^h - A X^h \|_2^2, \quad (11)$$

where μ is a nonnegative parameter, X^h is an $N \times 1$ column vector by reforming the two-dimensional horizontal edge information $\nabla_h^S T(x_i, y_j)$, the sparse transform D_f is usually exploited as a set of fixed bases such as the discrete cosine transform and wavelet, $D_f X^h$ denotes the discrete gradient of X^h at element $f (f = 1, 2, ..., N)$, and $\| \cdot \|_1$ and $\| \cdot \|_2$ stand for the l_1 norm and l_2 norm, respectively. We can get the vertical edge information $\nabla_v^S T(x_i, y_j)$ in the same way.

To compare the quality of the edge detection quantitatively, the SNR is used as an objective evaluation. We use the following definition in this evaluation[9–13]:

$$\mathrm{SNR} = \frac{\mathrm{mean}(T_{\mathrm{edge}}) - \mathrm{mean}(T_{\mathrm{back}})}{[\mathrm{var}(T_{\mathrm{back}})]^{0.5}}, \quad (12)$$

where T_{edge} and T_{back} are the intensity values of the edge detection results and background region, respectively, mean(·) represents the average value, and var(·) denotes the variance value. Next, we introduce the definition of a compression ratio:

$$\text{Compression ratio} = \frac{M}{m \times n} = \frac{M'}{m \times n \times L}, \quad (13)$$

where M is the number of speckle patterns, M' is the number of the measurements of the bucket detector, and m and n represent the horizontal and vertical dimensions of the object, respectively. Finally, L represents the number of the group of shifted speckle patterns using different operators. The L values for the gradient vector and Sobel operator algorithms are 2 and 8, respectively.

For comparison, numerical simulations and experiments detect the edge of a gray-scale object. Because of the randomness of the speckle patterns intensity distribution, we present the reconstructed image over 10 times in all of the following simulations and experiments, respectively, and the speckle patterns used in different methods of the same object are completely consistent. The simulations and experimental results (SNR) selected in the following paragraphs are the fifth of ten measurements of SNRs arranged in a small to large order, and we set μ equal to 2^{12} in Eq. (11) as a coefficient to balance the regularization and the data fidelity.

To evaluate the effectiveness of CGEI, we start with numerical simulations. The edge detection results of GGI coupled with a gradient vector of $\varphi = 45°$ (GGI-45°), SSGI coupled with a Sobel operator (SSGI-So), CGEI coupled with a gradient vector of $\varphi = 45°$ (CGEI-45°), and CGEI coupled with a Sobel operator (CGEI-So) are summarized in Fig. 2. There are 6554 speckle patterns (compression ratio: 0.4) modulated by DMD to illuminate the gray-scale objects (128×128 pixels). In the GGI scheme, GGI-45° is implemented with random patterns with two one-pixel-shifting, so the measurement of the bucket detector is twice the number of the random patterns (total 13,108 measurements). Similarly, the number of bucket detector measurements of the SSGI-So with eight one-pixel-shifting is eight times the number of random patterns (total 52,432 measurements), respectively. Meanwhile, the numbers of bucket measurements of the CGEI-45° and the CGEI-So are 13,108 and 52,432, respectively. The results in Fig. 2 show that CGEI enhances the ability of recognizing the target more than GGI-45° and SSGI-So. For "Picture1", the SNRs of edge detection using CGEI-45°, CGEI-So, GGI-45°, and SSGI-So are 5.2383, 10.0509, 0.6544, and 1.1592, respectively. The use of CGEI has an enhanced SNR of more than eight times. In addition, we also use "Picture2" as the target, and the simulation results are summarized in Fig. 2. Compared with the results of different schemes, we can see our scheme has consistently better SNR performance.

Next, we simulate the GGI-45°, SSGI-So, CGEI-45°, and CGEI-So processes with different compression ratios. The results (SNR) of different algorithms, as a function of measurements, where "Picture1" is the target, are shown in Fig. 3. We can see that the CGEI reconstruction is much better than GGI-45° and SSGI-So, regardless of the compression ratio.

There are a lot of various noises in the real world. According to Eq. (1), added white Gaussian noise (AWGN) is considered to simulate the bucket detection. The SNR of the bucket detector SNR_{BD} is defined as

$$\mathrm{SNR}_{BD} = 10 \log_{10} \frac{\mathrm{Power}_S}{\mathrm{Power}_N}, \quad (14)$$

where Power_S is the signal power collected by the bucket detector, and Power_N is the power of the AWGN with zero means imposed on the bucket detector. The resulting

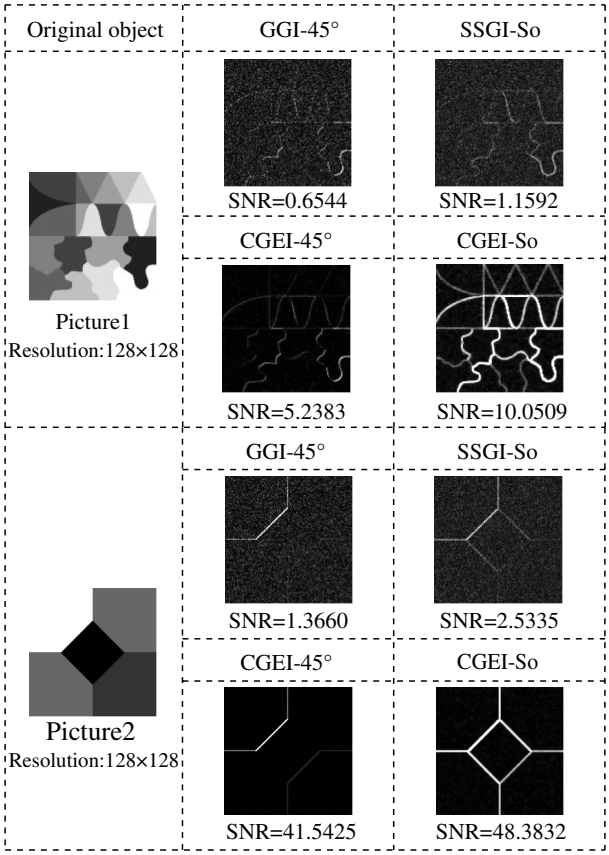

Fig. 2. Numerical simulation results of the unknown objects using different schemes, where SNR is presented together.

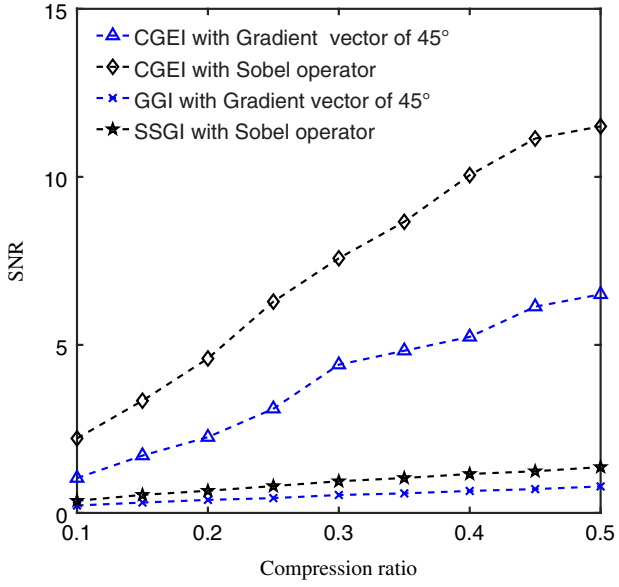

Fig. 3. Numerical simulation results (SNR) using different schemes for different compression ratios.

SNRs of different algorithms applied to "Picture1", where the number of speckle patterns is set to 4915 (compression ratio: 0.3), are shown in Fig. 4. From Fig. 4, we can see that as the power of the AWGN increases, the SNRs of

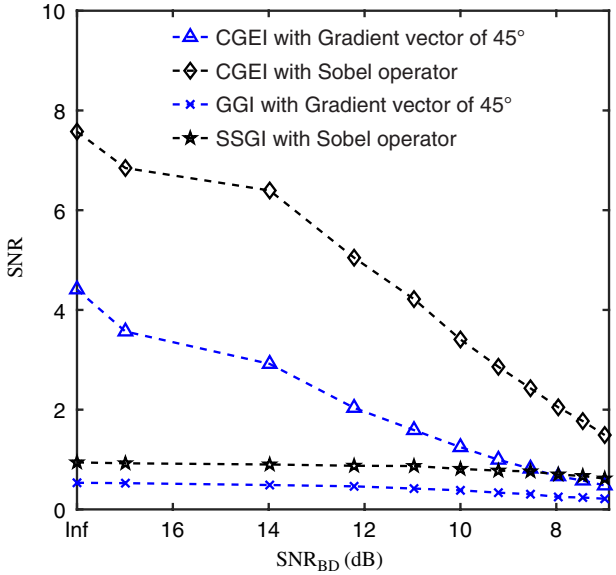

Fig. 4. SNR performance of edge information against SNR$_{BD}$ using different schemes.

the edge detection algorithms decrease. However, the CGEI method outperforms GGI-45° and SSGI-So when SNR$_{BD}$ is higher than 9 dB.

Moreover, we apply our scheme to data collected via an experiment. The prototype CGEI is shown in Fig. 5. One red LED is used as the source, and the light is collimated by lens L1 to be focused onto a DMD (DMD TIDLPC350). The DMD is controlled by a computer to modulate the light needed to generate the random speckle patterns, $S_k^l(x_i, y_j)$, $k = 1, 2, ..., M$. Later, the beams with the random speckle patterns are projected onto an object by lens L2. A rabbit doll (a gray-scale object) is used as the unknown object, which is shown in Fig. 5. The transmitted light carrying the object's scattering information is collected by an imaging lens L3 onto a bucket detector (Thorlabs PMM02) to complete the measurement. A pair of detection results ∇y_k^h and ∇y_k^v is recorded by the computer. Then, the edge of the object, organized as horizontal and vertical coordinates, are extracted by using the TVAL3 algorithm. Finally, we get the edge of the unknown object.

The experimental results are summarized in Fig. 6. The number of the speckle patterns is set to 2000 (compression ratio: 0.49). Similar to our theoretical analysis and simulations, we can see the edge detection method with the best performance. Thus, we can say that CGEI is better than GGI-45° and SSGI-So in real applications.

In addition, we also compare the experimental results (SNR) using different schemes for different compression ratios, and the results are shown in Fig. 7. In the figure, the rabbit is the object that needs to be reconstructed. Therefore, from Fig. 7, the experimental results show that CGEI outperforms other algorithms for different compression ratios.

To further illustrate the effectiveness of CGEI, we perform a simulation-based comparison. In most traditional

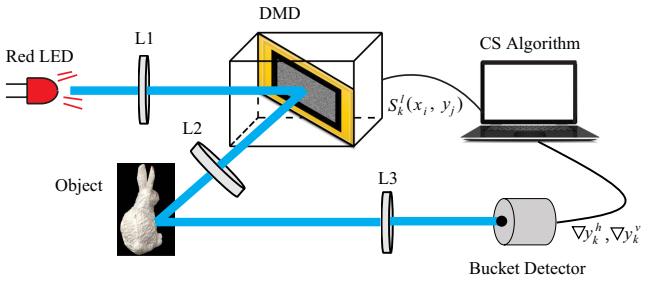

Fig. 5. Schematic diagram of the CGEI scheme experimental system.

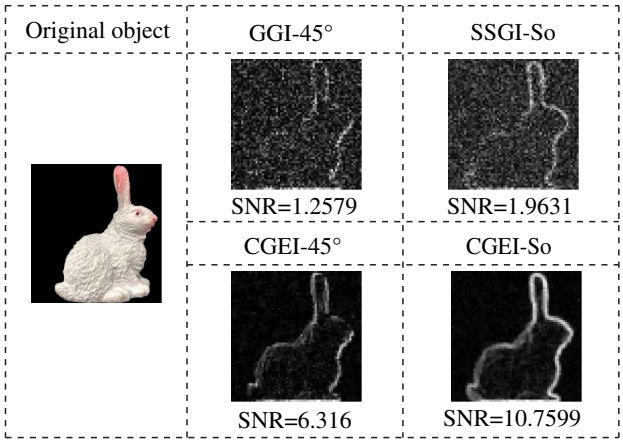

Fig. 6. Experimental results of the unknown object using different schemes, where SNR is presented together, and the resolution of results is 64×64.

edge detection approaches, the original target is imaged first, and the edge is extracted later (e.g., gradient vector-based and Sobel operator-based methods). In our

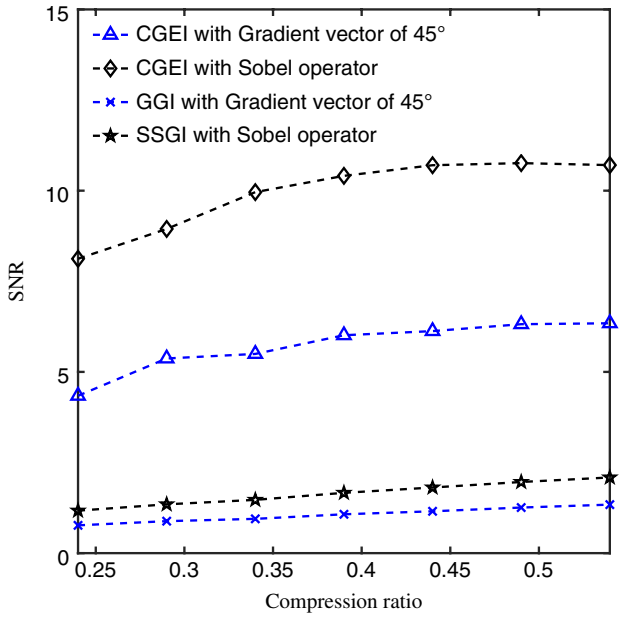

Fig. 7. Experimental results (SNR) using different schemes for different compression ratios.

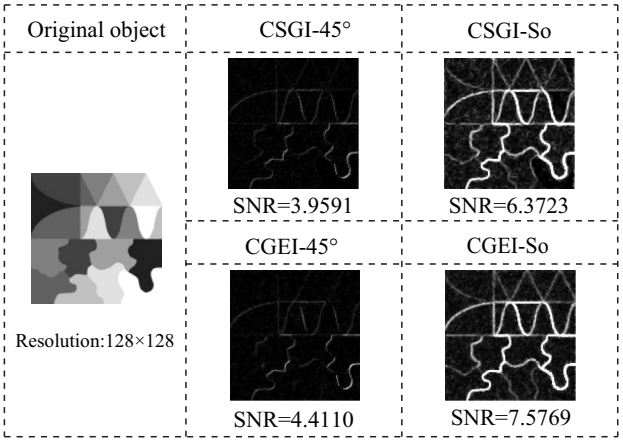

Fig. 8. Simulation results (SNR) of CSGI-45°, CSGI-So, CGEI-45°, and CGEI-So, where SNR is presented together.

simulation-based validation, we reconstruct the image of the object by using the CGI[16], and then use the gradient vector (CSGI-45°) and Sobel operator (CSGI-So) to extract the edge of an object from its image. The number of the speckle patterns is set to 4915 (compression ratio: 0.3). The SNRs of the reconstructed images are then reviewed. We find that the SNRs of CSGI-45° and CSGI-So are lower than that of CGEI-45° and CGEI-So, respectively; these results are shown in Fig. 8. Therefore, the simulation further illustrates the effectiveness of CGEI. In summary, CGEI can extract edge information from an unknown object without needing an image or priori information. Therefore, we dramatically improve the performance of an edge detection process by CGEI.

In conclusion, we have proposed an edge detection scheme by using CGEI in this Letter. We have compared the performance of GGI-45°, SSGI-So, CGEI-45°, and CGEI-So via numerical simulations and experiments. The results show that the imaging quality could be greatly improved by using CGEI (when compared to GGI-45° and SSGI-So). Moreover, we validate our results via a simulation that compares our methods, CGEI-45°, and CGEI-So to CSGI-45° and CSGI-So, respectively. The results further illustrate the effectiveness of CGEI. The simulations and experiments show that CGEI has good edge detection performance.

This work was supported by the National Natural Science Foundation of China (Nos. 61871234 and 11847062), the Postgraduate Research & Practice Innovation Program of Jiangsu Province (No. KYCX18_0900), the Natural Science Foundation of Jiangsu Province (BK20180755), the NUPTSF (No. NY218098), the Scientific Research and Innovation Team of Fuyang Normal University (No. kytd201706), and the Natural Science Research Project of Fuyang Normal University (No. 2015FXXZK02).

References

1. X. Xu, E. Li, X. Shen, and S. Han, Chin. Opt. Lett. **13**, 071101 (2015).
2. J. H. Shapiro, Phys. Rev. A **78**, 061802(R) (2008).

3. Y. Li, H. Yang, J. Liu, L. Gong, Y. Sheng, W. Cheng, and S. Zhao, Chin. Opt. Lett. **11**, 021104 (2013).
4. W. Wang, Y. P. Wang, J. Li, X. Yang, and Y. Wu, Opt. Lett. **39**, 5150 (2014).
5. Q. Li, Z. Duan, H. Lin, S. Gao, S. Sun, and W. Liu, Chin. Opt. Lett. **14**, 111103 (2016).
6. J. Cheng, Opt. Express **17**, 7916 (2009).
7. H. Zhao and M. Shang, Mod. Phys. Lett. B **32**, 1840088 (2018).
8. P. Arbeláez, M. Maire, C. Fowlkes, and J. Malik, IEEE Trans. Pattern Anal. Mach. Intell. **33**, 898 (2011).
9. X. F. Liu, X. R. Yao, R. M. Lan, C. Wang, and G. J. Zhai, Opt. Express **23**, 33802 (2015).
10. T. Mao, Q. Chen, W. He, Y. Zou, H. Dai, and G. Gu, IEEE Photonics J. **8**, 6900810 (2016).
11. L. Wang, L. Zou, and S. Zhao, Opt. Commun. **407**, 181 (2018).
12. S. Yuan, D. Xiang, X. Liu, X. Zhou, and P. Bing, Opt. Commun. **410**, 350 (2018).
13. H. D. Ren, S. M. Zhao, and J. Gruska, Opt. Express **26**, 5501 (2018).
14. X. Lin, N. Feng, Y. Qu, D. Chen, Y. Shen, and M. Sun, Chin. Opt. Lett. **15**, 101102 (2017).
15. Q. Guo, M. Chen, Y. Liang, H. Chen, S. Yang, and S. Xie, Chin. Opt. Lett. **15**, 010012 (2017).
16. O. Katz, Y. Bromberg, and Y. Silberberg, Appl. Phys. Lett. **95**, 131110 (2009).
17. V. Katkovnik and J. Astola, J. Opt. Soc. Am. A **29**, 1556 (2012).
18. H. Huang, C. Zhou, T. Tian, D. Liu, and L. Song, Opt. Commun. **412**, 60 (2018).
19. C. Li, W. Yin, H. Jiang, and Y. Zhang, Comput. Optim. Appl. **56**, 507 (2013).